

Hierarchical self-assembly for high-yield addressable complexity at fixed conditions

Miranda Holmes-Cerfon*

*Department of Mathematics, University of British Columbia
1984 Mathematics Rd, Vancouver, BC, V6T 1Z1, Canada*

Matthieu Wyart†

*Department of Physics and Astronomy
Johns Hopkins University, Baltimore, MD, USA
Institute of Physics*

*École Polytechnique Fédérale de Lausanne,
Lausanne, CH-1015, Switzerland*

(Dated: January 7, 2025)

There is evidence that the self-assembly of complex molecular systems often proceeds hierarchically, by first building subunits that later assemble in larger entities, in a process that can repeat multiple times. Yet, our understanding of this phenomenon and its performance is limited. Here we introduce a simple model for hierarchical addressable self-assembly, where interactions between particles can be optimised to maximise the fraction of a well-formed target structure, or yield. We find that a hierarchical strategy leads to an impressive yield up to at least five generations of the hierarchy, and does not require a cycle of temperatures as used in previous methods. High yield is obtained when the microscopic interaction decreases with the scale of units considered, such that the total interaction between intermediate structures remains identical at all scales. We provide thermodynamic and dynamical arguments constraining the interaction strengths where this strategy is effective. Overall, our work characterizes an alternative strategy for addressable self-assembly at a fixed temperature, and provides insight into the mechanisms sustaining hierarchical assembly in biology.

I. INTRODUCTION

The ribosome, the central machinery that translates messenger RNA into proteins, illustrates the surprising ability of multi-components systems to self-assemble. It is a protein complex made of ~ 100 proteins (in addition to ribosomal RNA), containing around 10^4 amino acids. Considering the astronomical number of possible configurations these amino acids could take, how does this system self-assemble correctly? Clearly, this process is simplified by the fact that amino-acids first fold into proteins, which later form a complex. There is evidence that such a hierarchical strategy, where small units first form before assembling into larger ones, is at play in the folding of individual proteins itself [1]. In this view, proteins first nucleate secondary structures such as beta sheets or alpha helices [2] or more complex "foldons" [3] which later organize into the full tertiary structure. Hierarchical self-assembly is also used in chemistry to obtain supra-molecular structures, typically held together with hydrogen bonds or Van der Waals interactions, much weaker than the covalent bonds organizing molecules [4]. More generally, a hierarchical organization is central to a variety of complex systems and processes, from engineering to the composition of companies from smaller entities [5]. Despite its importance and ubiquity, understanding the principles governing hierarchical assembly remains a

challenge.

Such principles could be used and tested in the context of "addressable" self-assembly, where each unit of a target structure is distinct and must assemble into a particular location [6–13]. Using DNA strands as building blocks with highly specific interactions, experimentalists have so realized highly complex structures containing up to tens of thousands of units [14–17]. A challenge is to find the particular building blocks [18] or protocols [19–21] such that the system assembles into a desired structure. Experiments operate in the regime where all pair interactions have roughly the same strength [22], although the importance of displaying a range of interactions has been proposed in various contexts [23, 24]. When these interactions are strong, or equivalently the temperature is low, the system assembles many partially-formed fragments of the target structures. These fragments must break apart to assemble into copies of the target structure, but they cannot do so on accessible timescales – although the target structure has the lowest free energy, it is not kinetically accessible. In contrast, with weaker interactions the target state no longer has the lowest free energy. One solution, identified experimentally and later rationalized theoretically [25, 26] is to anneal temperature: start at a high temperature where nucleation is rare, then slowly lower temperature to grow the nuclei, repeating until one forms a target structure. While this protocol has worked well as a method to form one or a small number of copies of a target structure, it wastes monomers, since many monomers do not assemble into a target structure, and furthermore it requires a precise temperature protocol.

* holmescerfon@math.ubc.ca

† matthieu.wyart@epfl.ch

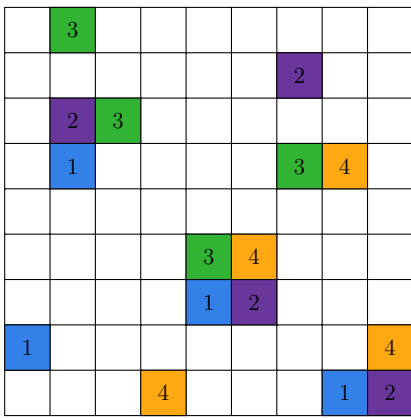


FIG. 1. Schematic of our model: particles on a square lattice interacting with pairwise energies. They move using the VMCM algorithm, which moves clusters as a unit with appropriate diffusivities. This schematic contains enough monomers to make four 4-squares. Only one 4-square has fully formed.

We wish to understand whether hierarchy can be used to achieve high-yield assembly at fixed conditions, without annealing. Most previous studies of hierarchical assembly required some kind of staged assembly, where the experimental conditions or protocols change with time [27–33], which is not always possible in biological contexts. A handful of recent studies have developed experimental systems that assemble via two stages of hierarchy at equilibrium [34–37]. This is often achieved using a mix of “strong” bonds, and “weak” bonds which become stronger due to geometric organization once the strong bonds have formed [38].

Here we introduce a minimal model of assembly at equilibrium, which we study up to five hierarchical steps. Our central results are that: (i) hierarchical assembly is possible in equilibrium, with fixed conditions; (ii) efficient assembly requires the scale of interaction to decrease with size, so that the binding energy of meta-particles is approximately independent of scale, (iii) the dynamics of self-assembly is itself hierarchical, the characteristic time at which meta-particles are formed scales with their length and (iv) we derive some constraints on the interaction strength for hierarchical self-assembly to properly occur, summarizing our results in a phase diagram.

II. HIERARCHICAL ASSEMBLY WITH STICKY SQUARES

A. Model

We consider a system of sticky squares (monomers) on a two-dimensional square lattice with periodic boundary conditions, as depicted in Fig. 1. We assume that monomer i interacts with monomer j with an interaction

energy 0 if the squares are not touching, ∞ if the squares overlap, and $-\delta_{ij}^{\vec{l}}$ if the squares are exactly touching with separation $\vec{l} \in \{(1, 0), (-1, 0), (0, 1), (0, -1)\}$. The target structure is an n -square containing $n = 2^k \times 2^k = 4^k$ monomers (Figure 2) where k is some integer, with each monomer in a distinct location. Our goal is to make N_c copies of this target structure at a constant temperature T . We measure interaction energies in units of $k_B T$ so the temperature will no longer enter our discussion. We simulate a collection of $N = nN_c$ monomers with interactions chosen such that $\delta_{ij}^{\vec{l}} > 0$ if i and j are copies of neighbouring monomers with separation \vec{l} in the target structure. We denote by ρ the concentration of any specified monomer, which is assumed equal for all monomers. All our simulations are run in a box with side length L and volume $V = L^2$, at volume fraction $\phi = N/V \approx 0.05$; note that $\phi = 4^k \rho$.

The dynamics is modeled using the Virtual Move Monte Carlo algorithm [39], whose equilibrium converges to the Boltzmann distribution, and which preserves many natural dynamical features when time is measured in Monte Carlo sweeps. Importantly, this algorithm allows moving clusters as a unit, merging clusters, and breaking apart clusters into sub-clusters. The average diffusion coefficient of a cluster may be a prescribed function of the cluster’s size or shape. We use an approximation to 3d Stokes’ drag, which implies a 4^k -square diffuses approximately with diffusion coefficient $D_k \approx 1/\sqrt{n} = 1/2^k$. To speed up the code, we enforce that monomers cannot rotate, which we expect not to change results qualitatively [40].

We aim to choose $\delta_{ij}^{\vec{l}}$ to make the system assemble hierarchically, and to explore when this makes the overall yield of the target structure high. We measure the yield y_k of 4^k -squares by the total number N_f of *perfectly formed* target structures, $y_k = N_f/N_c$, measured at a given time. We denote by $\Delta_k \equiv 1 - y_k$ the fraction of structures that do not correspond to the target.

B. Assembling 4-squares

We first study how elementary meta-particles, 4-squares, assemble. We set the native interaction energies to δ_1 (in units of $k_B T$) and all other interactions to 0. Fig. 3 shows the yield y_1 as a function of δ_1 at different times. At long times, the yield must approach its equilibrium value, the black dashed curve in Fig. 3 derived below. For a fixed time, the yield increases to a maximum at intermediate values of δ_1 , then decreases. The optimal yield increases with time, as does the value of δ_1 which produces it.

The decrease in yield at long times occurs because for large δ_1 , the system forms many fragments of three monomers (3-mers) as illustrated Fig. 3. The 3-mers must break apart to fit together into 4-squares, but doing so requires a long timescale $\sim e^{\delta_1}$ for large δ_1 . The

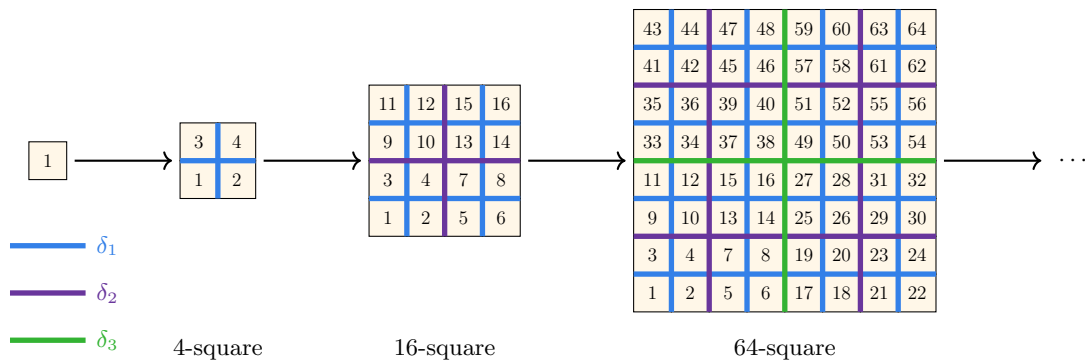


FIG. 2. Building large squares with addressable complexity using hierarchical interactions. Square monomers with sticky sides assemble into 4-squares with strong edge interactions δ_1 , 4-squares assemble into 16-squares with weaker individual edge interactions δ_2 , 16-squares assemble into 64-squares using even weaker edge interactions δ_3 , and so on. We expect good assembly when the interactions are chosen hierarchically $\delta_2 = \delta_1/2$, $\delta_3 = \delta_2/2$, $\delta_4 = \delta_3/2$, etc (for appropriate values of δ_1 , as studied below). This way, the energy for gluing together 4^k -squares into 4^{k+1} -squares, is the same as for gluing together monomers into 4-squares.

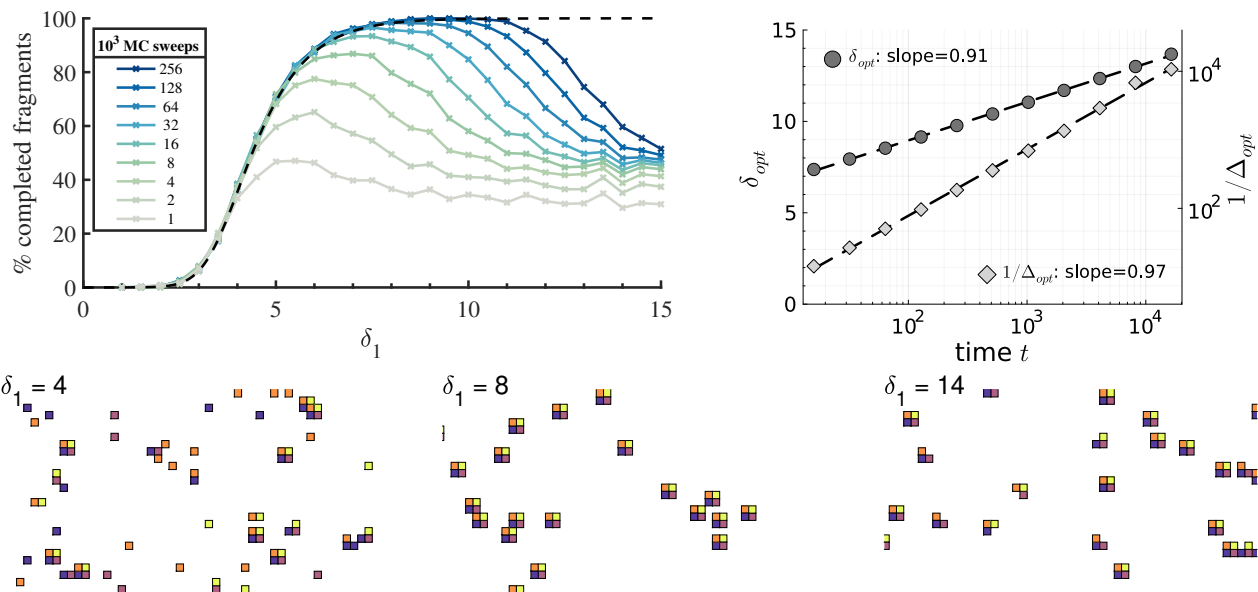


FIG. 3. Building 4-squares with varying side energies δ_1 . Top left: the percentage of fully-completed 4-squares from simulations at different times (markers/solid lines). Black dashed line shows the equilibrium fraction of 4-squares, from Eqn. (A4). Simulations considered $N_c = 100$, $L = 89$, and for each δ_1 were repeated 12 times to obtain an average yield. Bottom: snapshots of individual simulations after 128 MC sweeps, showing about 1/9th of each system. For small δ_1 , the system is in equilibrium and contains a mixture of fragment sizes. For medium δ_1 , the system is nearly 100% 4-squares. For large δ_1 , the system forms a mixture of 3-mers and 4-squares. The 3-mers cannot fit together to form 4-squares without breaking apart, which happens on a longer timescale, so the system is kinetically trapped. Top right: the optimal interaction energy δ_{opt} which maximizes $c_4(t)$, the concentration of 4-squares at time t , and the corresponding inverse fraction of errors $\Delta_{\text{opt}}^{-1}(t) = (1 - c_4(t)/\rho)^{-1}$, found by solving nonlinear rate equations (B1) at $\phi = 0.05$. Dashed lines are the best-fit lines on a log-linear and log-log scale respectively; their slopes are shown in the legends and are in good agreement with the unit slopes predicted by Eqns. (2), (3).

system is kinetically trapped at intermediate times.

Theory: An exact formulation of the thermodynamics and kinetics of the formation of 4-squares is presented in the SI. Here we emphasize key facts. In the regime of high yield, the dominant species at equilibrium is the fully formed 4-squares of concentration c_4 , followed by individual monomers of concentration c_1 . Thus the de-

crease in yield is $\Delta_1 \approx c_1/\rho$ while $c_4 \approx \rho$. Imposing that the reaction whereby 4 single monomers form a 4-square satisfies detailed balance leads to $c_1 = e^{-\delta_1} c_4^{1/4}$, which implies:

$$\Delta_1 \approx e^{-\delta_1} \rho^{-3/4}. \quad (1)$$

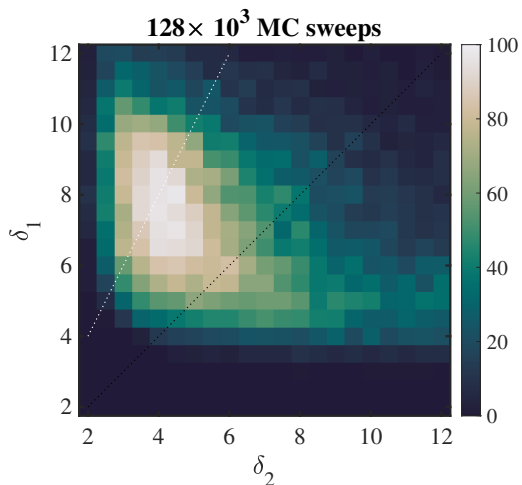


FIG. 4. Building 16-squares with varying side energies δ_1, δ_2 . Colors show the percentage of fully-completed 16-squares after 128×10^3 MC sweeps. The average yield is nearly 100% for a range of energies near $\delta_1 = 2\delta_2$ (white dotted line), while the yield is notably worse for identical interactions $\delta_1 = \delta_2$ (black dotted line). Simulations considered $N_c = 10$ copies of a 16-square, and for each value of (δ_1, δ_2) were repeated 12 times to obtain an average yield.

Two time scales govern the kinetics of the assembly process: the diffusion time for monomers to meet, $\tau_D \sim (D_0\rho)^{-1}$, and the unbinding time for a bond to break, $\tau_B \sim e^{\delta_1}/D_0$ (recall D_0 is the diffusion coefficient of a monomer). When the ratio $f \equiv \tau_B/\tau_D = e^{\delta_1}\rho$ is large, the concentration c_3 of triangles remains large (of order ρ) during the assembly process, whose duration is of order τ_B . This effect is apparent at the bottom of Fig.3, where an abundance of triangles is visible at the considered time scale. As we shall see below, this situation is detrimental in the hierarchical assembly, as it can lead to the presence of defects. For 4-squares it is not an issue: if ρ is fixed and one is given a large time t to assemble, then the optimal yield is obtained by choosing δ_1 such that $\tau_B \sim t$, corresponding to

$$\delta_1 \approx \ln(D_0 t). \quad (2)$$

This leads to an error that decreases rapidly with the assembly time, as $\Delta_1 \sim 1/(t\rho^{3/4})$ or equivalently:

$$\Delta_1^{-1} \approx D_0 t \rho^{3/4}. \quad (3)$$

To test the time-dependence of these two scaling laws, we compute the value of δ_1 which optimizes the concentration of 4-squares at different times t , by solving nonlinear rate equations for the different structures entering the assembly process (SI Secion B). The predicted scaling laws with t are confirmed in Fig.3.

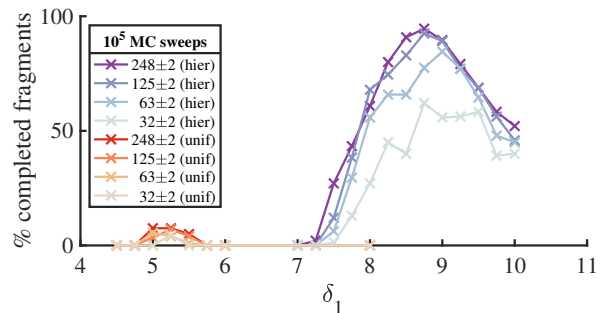


FIG. 5. Yield of perfect 256-squares in simulations of $N_c = 4$ copies of a 256-square, initialized as a gas. Purple colours show the average yields at varying times as indicated in color using hierarchical energies ($\delta_1=2\delta_2=4\delta_3=8\delta_4$), and red colours show the average yields using uniform energies ($\delta_1=\delta_2=\delta_3=\delta_4$). Simulations for each δ_1 were repeated 12 times for hierarchical interactions, and 10 times for uniform interactions.

C. Assembling 16-squares is best done using hierarchical interactions

Since we can make 4-squares for a range of interaction energies, we now ask whether we can glue these 4-squares together in the same arrangement to form 16-squares, using the same overall interaction energies that we used for the monomers in the 4-squares. If we used interaction energy δ_1 to make 4-squares, and we wish the overall interaction energy between 4-squares to also be δ_1 , then interactions between sides of monomers that are native to the 16-square but that are not in a 4-square must be $\delta_2 = \delta_1/2$ (Figure 2).

We explore whether this intuition is correct by varying the interaction energies δ_1, δ_2 for a system of 16-squares (Figure 4). The highest average yield after a given fixed time is 97.5%, for $(\delta_1, \delta_2) = (8, 4.5)$. The yield is not sensitive to these parameters: it is above 90% for a selection of parameters roughly in the range $(\delta_1, \delta_2) \in [6.5, 8.5] \times [3.5, 5]$. This is near the line $\delta_2 = \delta_1/2$, validating our hypothesis that hierarchical interactions should lead to efficient assembly. It is notable that uniform interaction energies ($\delta_1 \approx \delta_2$) never lead to such high yield over the time scales considered – the highest uniform yield is 82.5% for $\delta_1 = \delta_2 = 6$, but most yields are much smaller.

D. Assembling n -squares with high yields via hierarchical interactions

We now apply this principle of choosing interactions in a self-similar manner to build larger objects. The largest system we can explore systematically is a 256-square, which requires additional side energies $\delta_3 = \delta_2/2$ to make the intermediate 64-squares, and $\delta_4 = \delta_3/2$ to make the final 256-squares, as illustrated in Fig.2. Fig.5 com-

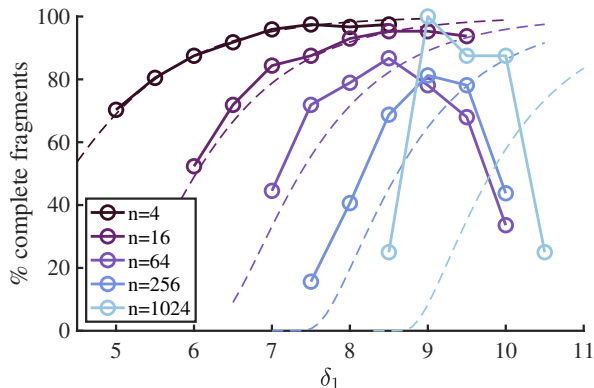


FIG. 6. Yields of $n=4^k$ -squares using hierarchical interactions (markers/solid lines), as a function of strongest interaction energy δ_1 , calculated at times increasing by a factor of 8 for each generation (except for $k=5$ as described in the text). Dashed lines correspond to equilibrium approximation Eq.4.

compares the yield of a 256-square with both hierarchical and uniform interactions, as a function of δ_1 . The yield with hierarchical interactions reaches 95% at late times with $\delta_1=8.75$, but is notably high over a broad range of timescales and a range δ_1 values spanning about $2k_B T$; the yield is not sensitive to the particular choices of parameters. In contrast, the maximum yield for uniform interactions over this timescale is only 8%; this occurs near $\delta_1=5$ for a narrow range of interaction energies spanning about $0.5k_B T$.

As a check that we can extend hierarchical assembly by one more generation we simulated $N_c = 2$ copies of a 1024-square using $\delta_1=10$, for a time of 1.15×10^6 MC sweeps, and repeated 4 times. Out of the 8 total copies of a 1024-square simulated, 7 copies formed perfectly, and 1 copy was missing two monomers from its interior. Snapshots of a perfectly-assembling system are shown in S.I., Fig. 13.

Hierarchical assembly as the number of generations k varies is compared in Fig.6. To choose the duration of these runs systematically, we consider $k = 1$ and determine a time $t_1 = 64 \times 10^3$ MC sweeps at which y_1 is close enough to equilibrium over a range of δ_1 values. For larger k , we chose $t_k = 8^{k-1}t_1$, based on scaling time with the diffusion timescale for each generation, $\tau_D^k = (D_k \rho)^{-1}$ (for each subsequent generation, ρ decreases by a factor of 4 for fixed volume fraction ϕ , and D_k decreases by a factor of 2). Generation $k = 5$ is run for about half that time because of computational limitations.

Fig. 6 shows that the yields are high over a range of δ_1 -values for all generations, though they decrease slightly with each new generation as explained below. An exception is $k = 5$ which has abnormally high yields, which we attribute to finite-size effects (Fig. 14; SI Section C 2). The curves appear shifted to the right by about $1k_B T$ for each additional generation. This is consistent with (1), which shows that for fixed error rate Δ_1 in the first gener-

ation and fixed volume fraction $\phi = 4^k \rho$, the interaction energy must increase by about $3/4 \log 4 \approx 1.04k_B T$ for each additional generation (see also SI, (A7)).

The yield curves must eventually go down with interaction strength, as already apparent for $k \geq 3$ for the range of interaction strengths considered. Upon visual inspection, we see small vacancy defects in target structures formed with larger k and δ_1 . We will study systematically this point below.

E. Dynamics of hierarchical assembly

Fig.7 illustrates via snapshots the comparison between hierarchical (top) and regular (bottom) assembly. The difference is visually striking: for the hierarchical assembly, fragments often consist of completed meta-squares with flat boundaries. By contrast, regular self-assembly is more similar to crystal growth, where shapes with rough boundaries appear.

This difference in the assembly pathways can be further probed by studying the mass distribution in fragments of different sizes as a function of time (Figure 8). For hierarchical interactions, most mass at early times is concentrated in fragments of size 1, then 4, then 16, then 64, with most remaining mass in multiples of these sizes (8,12, 32, 48, 128, 192). For uniform interactions, the system mass is concentrated in fragments of size 1, and of sizes near but slightly less than 256, with very little mass in between. Individual growth trajectories in the mass plots resemble random walks in the space of fragment size, with a bias toward larger sizes. This feature is not present with hierarchical interactions.

To quantify this behaviour further, in the top panel of Fig.9 the mass in fragments of size $n = 4, 16, 64, 256$ is shown as a function of time, for a system of assembling 256-squares with optimal hierarchical interactions. The peaks in the masses occur at subsequently increasing times and then decay, except for the targeted structure $n = 256$. Noticeably, the decaying parts of the curves appear simply shifted in time by $1/\sqrt{n}$ as n increases, consistent with scaling the decay with the diffusion timescales as we rationalize below.

III. CONSTRAINTS ON HIERARCHICAL ASSEMBLY

We have shown that hierarchical assembly pathways may be created by choosing appropriate interaction strengths, and they can lead to efficient, high-yield assembly. We now consider the conditions under which such assembly will be successful, considering both thermodynamic and kinetic constraints.

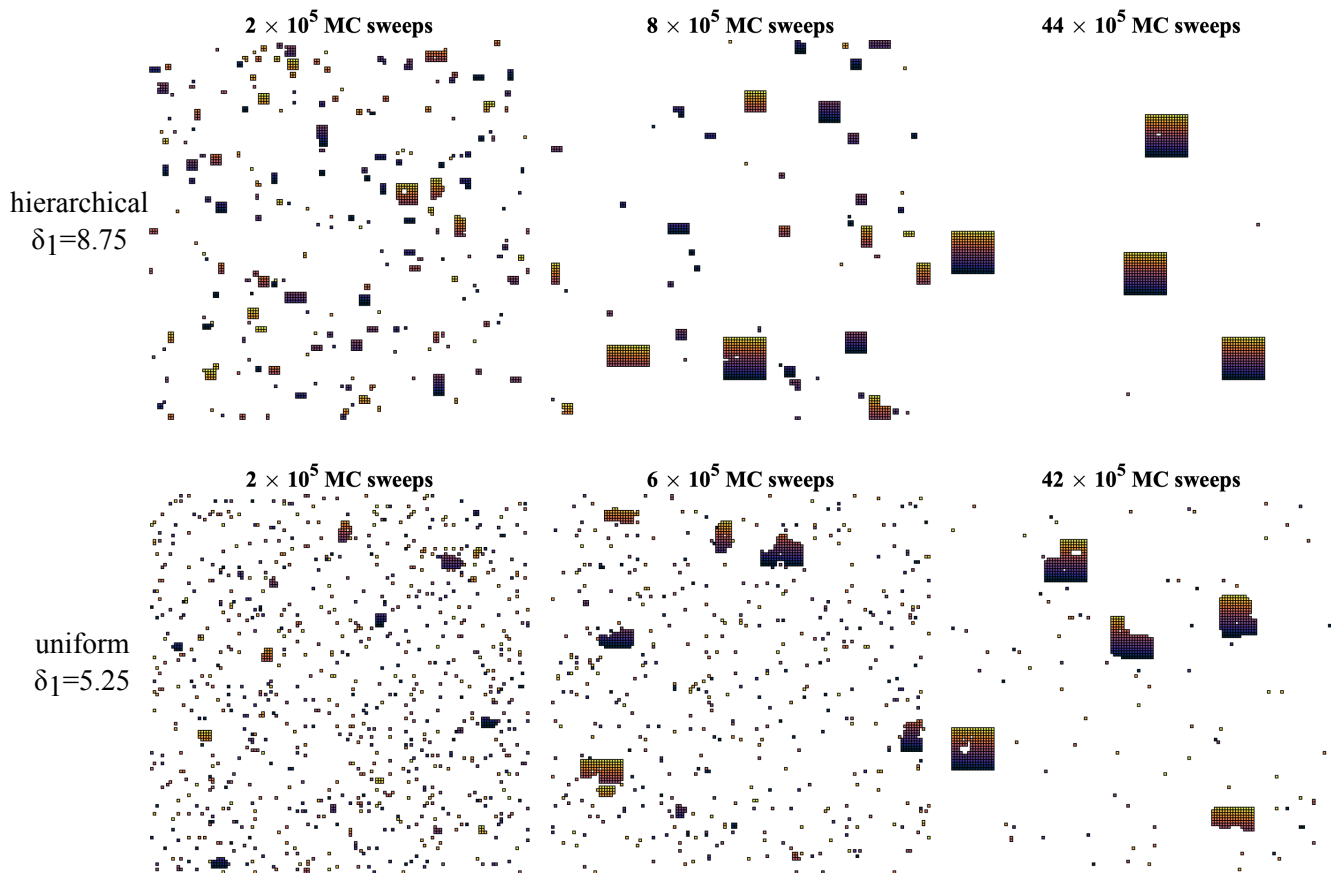


FIG. 7. Snapshots of individual simulations of assembling 256-squares at the best-assembling interaction energies: hierarchical ($\delta_1 = 8.75$, top) and uniform ($\delta_1 = 5.25$, bottom).

A. Thermodynamics constraints

We seek to estimate the yield y_k of hierarchical self-assembly with k generations, as a function of the monomer density ρ and of the interaction strengths. Let us denote by $\tilde{\delta}_j = 2^j \delta_j$ the effective interaction between two fully formed squares at the j^{th} intermediate generation, each consisting of 4^j monomers. We will assume that $\tilde{\delta}_j = \delta$ independently of j . We denote by $y_j^{(k)}$ the yield of such squares. At the first generation, assuming that weaker interactions do not disturb the kinetic of the assembly process (see below), from Eq.1 we get $y_1^{(k)} = 1 - \Delta_1(\rho)$. We can now proceed recursively, assuming that (i) the formation of squares at generation j is not affected by that of larger structures and (ii) that it only depends on the concentration of $j - 1$ squares obtained in the process, which only depends on the yields of previous stages j' with $1 \leq j' \leq j$. The yields of intermediate generations are thus approximated as

$$y_j^{(k)}(\rho) = y_{j-1}^{(k)}(\rho) y_1^{(k)}(\rho y_{j-1}(\rho)), \quad (4)$$

and the target yield $y_k = y_k^{(k)}$ is computed recursively. This yield approximation is tested against simulation

data in Fig.6 (dashed lines). It correctly captures the trend for the yield, and even agrees quantitatively for weak interactions and small k .

Since a final yield of order unity requires a high yield already at the first generation, Eq.1 implies

$$e^\delta \gg \rho^{-3/4}. \quad (5)$$

Thus the thermodynamic yield increases with δ . However, for large enough δ kinetic effects drastically reduce the yield, as we now discuss.

B. Kinetic constraints

Bonds must have time to detach to avoid misfits: The assembly time must be larger than the time it takes any interaction to detach. Since the unbinding timescale for generation j , $\tau_B^j \sim e^\delta / D_j$, is largest for the final generation, this implies:

$$t \gg e^\delta / D_k. \quad (6)$$

Remaining hierarchical: For hierarchical assembly to proceed, interactions needed to build the generation $j+1$

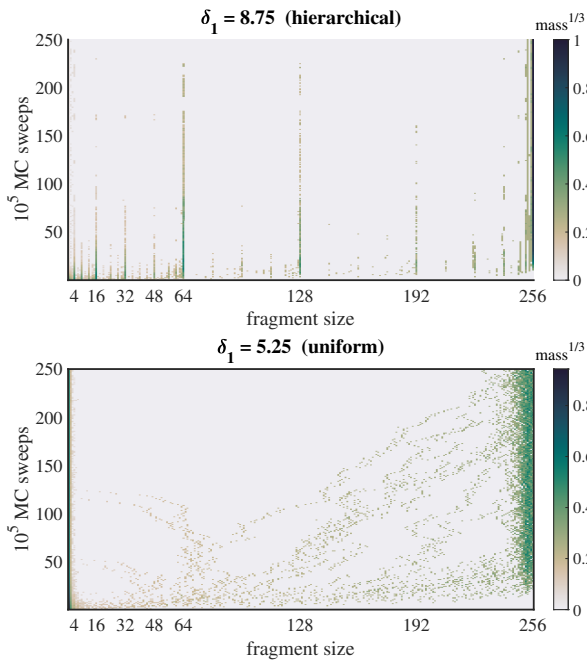


FIG. 8. The mass distribution of fragments of varying size (x axis) as a function of time (y axis) as indicated in color, for the simulations described in Fig. 5. Parameters correspond to the best-assembling hierarchical energy ($\delta_1 = 8.75$, top), and the best-assembling uniform energy ($\delta_1 = 5.25$, bottom). For hierarchical interactions, most mass lies in fragments of sizes 4, 16, 64, and finally 256, with some mass also in multiples of these sizes. For uniform interactions, individual growth trajectories appear in the mass plot, consistent with the notion that clusters grow by adding monomers one by one. The color scheme is $\text{mass}^{1/3}$ to highlight low-mass details.

should not interfere with the assembly of generation j ; they should start to play a role only when the j -squares are fully formed. Uncompleted substructures (such as triangles) of two adjacent j -squares bind with an interaction $\delta/2$. They will thus stick together even when the j squares are not completed, and remain attached for some time $\sim e^{\delta/2}/D_j$. If this time is much larger than the diffusion time $\tau_D^j \sim 1/(\rho D_j)$ for j -squares to meet, then partially formed structures spend most of their time bound to other partially formed structures. Proper hierarchical assembly can only happen when this does not occur, implying:

$$e^{\delta/2} \ll \frac{1}{\rho}. \quad (7)$$

Avoiding defects: As discussed for the formation of 4-squares, the concentration of triangles will be abundant at any level j at some point during the hierarchical assembly if the ratio of unbinding time over diffusion time $f^j \equiv \tau_B^j/\tau_D^j = e^\delta \rho$ is large. If the associated condition $f^j \gg 1$ or equivalently:

$$e^\delta \gg \frac{1}{\rho} \quad (8)$$

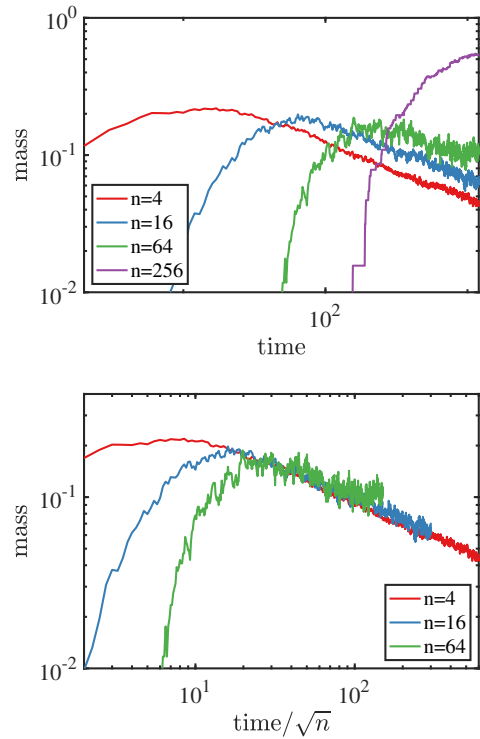


FIG. 9. (Top) Fraction of the system mass in fragments of size $n = 4, 16, 64, 256$, for a system of $N_c = 16$ 256-squares with $\delta_1 = 8.75$, repeated 8 times. (Bottom) Same data but with time rescaled by $1/\sqrt{n}$.

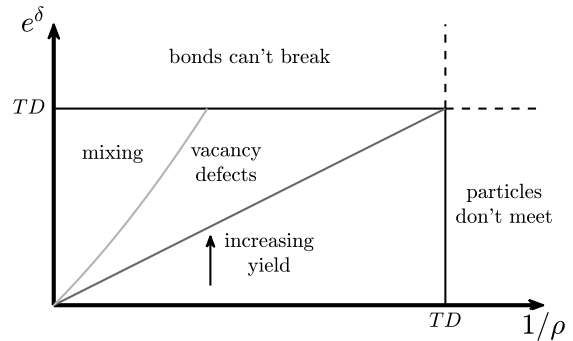


FIG. 10. A schematic phase diagram for hierarchical assembly.

holds, we expect to see defects composed of a triangle binding to three completed squares, such that an inaccessible hole is present in the interior of this structure. Indeed, the energy of removing the triangle to heal such a defect is precisely δ ; condition Eq.8 ensures that the healing time is smaller than the characteristic time where intermediate structures meet and bind.

Interestingly, if we denote by t_j the time scale to form generation j , we have that t_j is always inversely proportional to D_j . Indeed, t_j corresponds to the slowest time between the unbinding time τ_B^j and the diffusion time

τ^j , and both satisfy this property. Since $D_j \sim 1/\sqrt{4^j}$, one expects that during the hierarchical assembly, subsequent generations should take 2 times longer to form. Thus, $t_j \sim 2^j \sim \sqrt{n}$, as confirmed in Fig.9.

C. Phase diagram

Our results are summarized in the phase diagram of Fig. 10, with snapshots from different regions of the diagram shown in Fig. 11. At fixed ρ , at low δ the yield is poor as expected thermodynamically, and improves continuously as δ increases. For $e^\delta > C/\rho$ (here C represents an unknown constant), defects can start to appear. For even stronger interactions $e^\delta > C/\rho^2$, the notion of hierarchical assembly is lost, as interactions associated with different levels can bind concomitantly. Finally for $e^\delta > CtD$, low-level bonds have no time to detach: kinetic traps appear already at small scales.

Overall, we expect that yield is governed by a trade-off between thermodynamics, which favors large δ , and defect formation, so that optimality is reached near the regime where defects appear, i.e. for e^δ not too large in comparison with $1/\rho$. However, at that stage structures are still formed, but with a few defects. Thus, if a more relaxed definition of yield that includes structures with a small number of defects is considered, we expect that this optimal relaxed yield is obtained for larger δ . This view is supported by Fig. 12, comparing the yield (left panel) with a relaxed definition of yield, which indeed peaks at a larger δ (Fig. 12).

IV. CONCLUSION

The dominant protocol for high yield addressable self-assembly is based on heterogeneous nucleation: start from high temperature where nucleation is rare so that forming structures do not compete, and eventually lower temperature to make the structure form with fewer defects. Biology however offers examples of self-assembly with high yield at a fixed temperature, raising the possibility that other interaction designs may display higher yields. We have introduced a simple model to illustrate that hierarchical self-assembly is a powerful design principle for the interaction pattern, leading to very high yield. In this case, the dynamics is markedly different from heterogeneous nucleation. Particles first assemble into sub-

units, themselves forming units and so on in a sequential manner, instead of displaying structures whose masses continuously grow.

We have established that for hierarchical self-assembly, various quantities scale with the mass m of sub-structures considered. On the one hand, pairwise interaction should decrease at the boundary of large units, such that structures at a given scale display an overall interaction independent of that scale. For compact sub-structures that fill up space, this implies a microscopic interaction strength decreasing as $m^{(d-1)/d}$ where d is the spatial dimension. We argued that the optimal interaction strength δ will satisfy $C_1/\rho \leq e^\delta \leq C_2/\rho^2$, the first inequality marking where defects starts to increase, and the second where hierarchical assembly breaks down as generations do not grow sequentially. Determining quantitatively the precise location where yield is optimal for a given assembly duration remains a theoretical challenge for the future. Overall, although our predictions are verified in a simple model of sticky squares, we expect them to apply in more general situations, including with DNA bricks where they could be tested.

Our analysis also suggests to revisit the role of hierarchical assembly in protein folding. Folding is believed to occur successfully because the energy landscape presents a funnel shape [41], a description that however does not distinguish between very distinct folding mechanisms. Multiple mechanistic views exist, ranging from pure nucleation [42] to hierarchical folding [1, 2] as well as intermediary scenarios including both phenomena acting at different scales [3]. Studying this question would require to extend our analysis to the case where monomers come from a finite set, and are constrained to form a chain. Interestingly, this problem may become experimentally accessible in soft matter systems, for which chains of particles with specific interactions can be built [33].

ACKNOWLEDGMENTS

We thank J. Brujic, M. Johnson, D. Gracias, A. Grosberg and R. Schulman for discussions. M.W acknowledges support from the Simons Foundation Grant (No. 454953 Matthieu Wyart). M.H.C. acknowledges support from the Alfred P. Sloan Foundation, and from the Natural Sciences and Engineering Research Council of Canada (NSERC), RGPIN-2023-04449 / Cette recherche a été financée par le Conseil de recherches en sciences naturelles et en génie du Canada (CRSNG).

[1] K. A. Dill, S. B. Ozkan, M. S. Shell, and T. R. Weikl, *Annu. Rev. Biophys.* **37**, 289 (2008).
 [2] R. L. Baldwin and G. D. Rose, *Trends in biochemical sciences* **24**, 26 (1999).
 [3] A. R. Fersht, *Current opinion in structural biology* **7**, 3 (1997).

[4] J. A. Elemans, A. E. Rowan, and R. J. Nolte, *Journal of Materials Chemistry* **13**, 2661 (2003).
 [5] H. A. Simon, *Proceedings of the American philosophical society* **106**, 467 (1962).
 [6] P. W. K. Rothmund and E. S. Andersen, *Nature* **485**, 584 (2012).

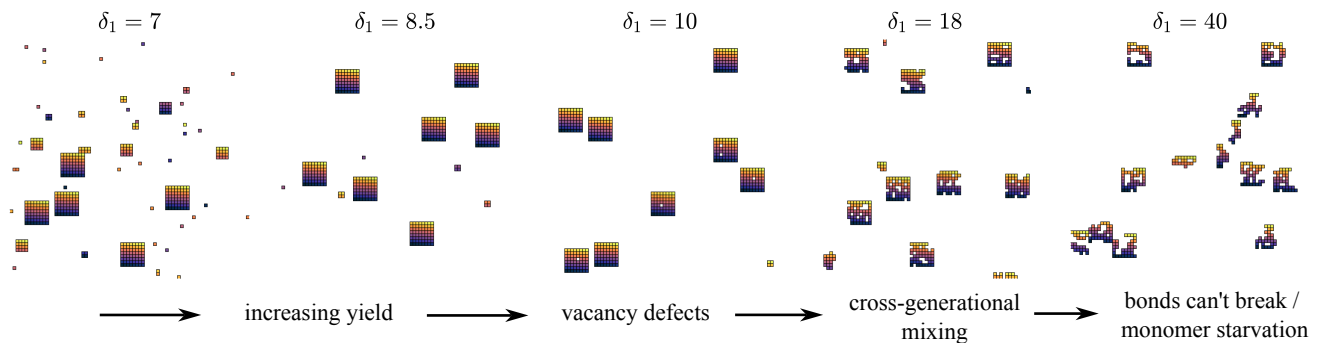


FIG. 11. Snapshots showing qualitatively how hierarchical assembly behaves as δ_1 increases, for $n = 64$ at fixed volume fraction ϕ . This corresponds to moving upwards along a vertical line in the phase diagram in Fig. 10. The examples are taken from simulations described in Fig. 12, and are plotted at $t = 256$ (time units are described in the caption to Fig. 12).

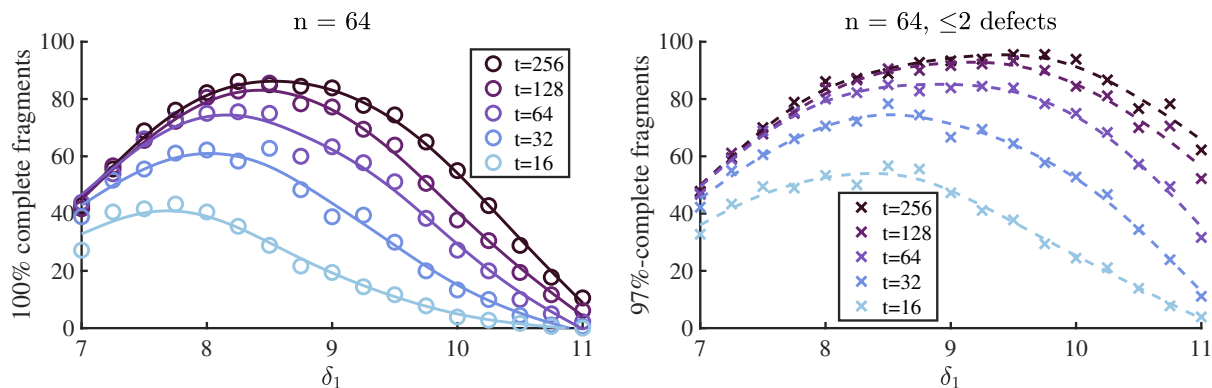


FIG. 12. Detailed simulations of 64-square assembly. Left: yield of perfectly-formed 64-squares at different times and different δ_1 -values from simulations (markers), and a spline curve fit through each set of data to show the trend (solid curves). Left: same, but the yield includes structures with at most 2 monomers missing (markers), with spline curves (dashed lines). For each value of δ_1 , simulations considered 60 copies of a 64-square, repeated 3 times, at volume fraction $\rho = 0.05$. Time is measured in units of 32×10^3 MC sweeps.

- [7] P. W. K. Rothmund, *Nature* **440**, 297 (2006).
- [8] S. Sacanna, D. J. Pine, and G.-R. Yi, *Soft Matter* **9**, 8096 (2013).
- [9] Y. Wang, Y. Wang, D. R. Breed, V. N. Manoharan, L. Feng, A. D. Hollingsworth, M. Weck, and D. J. Pine, *Nature* **491**, 51 (2012).
- [10] W. B. Rogers and V. N. Manoharan, *Science* **347**, 639 (2015).
- [11] W. B. Rogers, W. M. Shih, and V. N. Manoharan, *Nature Reviews Materials* **1**, 16008 (2016).
- [12] F. Hong, F. Zhang, Y. Liu, and H. Yan, *Chemical Reviews* **117**, 12584 (2017).
- [13] A. Murugan, Z. Zeravcic, M. P. Brenner, and S. Leibler, *Proceedings of the National Academy of Sciences* **112**, 54 (2015).
- [14] B. Wei, M. Dai, and P. Yin, *Nature* **485**, 623 (2012).
- [15] Y. Ke, L. L. Ong, W. M. Shih, and P. Yin, *Science* **338**, 1177 (2012).
- [16] L. L. Ong, N. Hanikel, O. K. Yaghi, C. Grun, M. T. Strauss, P. Bron, J. Lai-Kee-Him, F. Schueder, B. Wang, P. Wang, J. Y. Kishi, C. Myhrvold, A. Zhu, R. Jungmann, G. Bellot, Y. Ke, and P. Yin, *Nature* **552**, 72 (2017).
- [17] C. G. Evans, J. O'Brien, E. Winfree, and A. Murugan, *Nature* **625**, 500 (2024).
- [18] E. M. King, C. X. Du, Q.-Z. Zhu, S. S. Schoenholz, and M. P. Brenner, *Proceedings of the National Academy of Sciences* **121**, e2311891121 (2024).
- [19] C. P. Goodrich, E. M. King, S. S. Schoenholz, E. D. Cubuk, and M. P. Brenner, *Proceedings of the National Academy of Sciences* **118**, e2024083118 (2021).
- [20] A. Bupathy, D. Frenkel, and S. Sastry, *Proceedings of the National Academy of Sciences* **119**, e2119315119 (2022).
- [21] M. C. Engel, J. A. Smith, and M. P. Brenner, *Physical Review X* **13**, 041032 (2023).
- [22] S. Hormoz and M. P. Brenner, *Proceedings of the National Academy of Sciences* **108**, 5193 (2011).
- [23] A. Jhaveri, S. Loggia, Y. Qian, and M. E. Johnson, *Proceedings of the National Academy of Sciences* **121**, e2403384121 (2024).
- [24] R. Kaplan, J. Klobošický, S. Pandey, D. H. Gracias, and G. Menon, *Artificial life* **20**, 409 (2014).
- [25] A. Reinhardt and D. Frenkel, *Physical Review Letters* **112**, 238103 (2014), 1402.6228.
- [26] W. M. Jacobs, A. Reinhardt, and D. Frenkel, *Proceedings of the National Academy of Sciences* **112**, 6313

- (2015), 1502.01351.
- [27] S. H. Park, C. Pistol, S. J. Ahn, J. H. Reif, A. R. Lebeck, C. Dwyer, and T. H. LaBean, *Angewandte Chemie* **118**, 6759 (2006).
- [28] M. Grunwald and P. L. Geissler, *ACS Nano* **8**, 5891 (2014).
- [29] S. Whitelam, *Soft Matter* **11**, 8225 (2015).
- [30] W. Pfeifer and B. Saccà, *ChemBioChem* **17**, 1063 (2016).
- [31] K. F. Wagenbauer, C. Sigl, and H. Dietz, *Nature* **552**, 78 (2017).
- [32] Y. Zhang, A. McMullen, L.-L. Pontani, X. He, R. Sha, N. C. Seeman, J. Brujic, and P. M. Chaikin, *Nature Communications* **8**, 1 (2017).
- [33] A. McMullen, M. Muñoz Basagoiti, Z. Zeravcic, and J. Brujic, *Nature* **610**, 502 (2022).
- [34] R. Freeman, M. Han, Z. Álvarez, J. A. Lewis, J. R. Wester, N. Stephanopoulos, M. T. McClendon, C. Lynsky, J. M. Godbe, H. Sangji, *et al.*, *Science* **362**, 808 (2018).
- [35] O. G. Hayes, B. E. Partridge, and C. A. Mirkin, *Proceedings of the National Academy of Sciences* **118**, e2106808118 (2021).
- [36] J. Zou, A. C. Stammers, A. Taladriz-Sender, J. M. Withers, I. Christie, M. S. Vega, B. L. Aekbote, W. J. Peveler, D. A. Rusling, G. A. Burley, and A. W. Clark, *ACS Nano* **17**, 752 (2023).
- [37] Y. Jiang, M. S. Pacella, S. Lee, J. Zhang, J. A. Gunn, P. Vallejo, P. Singh, T. Hou, E. Liu, and R. Schulman, *Nanoscale* **16**, 11688 (2024).
- [38] F. M. Gartner and E. Frey, *Physical Review X* **14**, 021004 (2024).
- [39] S. Whitelam and P. L. Geissler, *The Journal of Chemical Physics* **127**, 154101 (2007).
- [40] C. G. Evans and E. Winfree, *Chemical Society Reviews* **46**, 3808 (2017).
- [41] J. D. Bryngelson, J. N. Onuchic, N. D. Socci, and P. G. Wolynes, *Proteins: Structure, Function, and Bioinformatics* **21**, 167 (1995).
- [42] N. V. Dokholyan, S. V. Buldyrev, H. E. Stanley, and E. I. Shakhnovich, *Journal of molecular biology* **296**, 1183 (2000).

SUPPLEMENTARY INFORMATION

Appendix A: Equilibrium calculations, details

This section contains a few details supporting the calculations in Section III A of the main text.

First suppose we wish to make a 4-square, and consider all the intermediate fragment types: there are 4 types of monomers with energy 0, 4 types of 2-mers with energy $-\delta$, 4 types of trimers with energy -2δ , and 1 type of 4-mer with energy -4δ . Let n_i be the total number of i -mers observed, and let c_i be the concentration of each type of i -mer, so that $c_1 = n_1/4V$, $c_2 = n_2/4V$, $c_3 = n_3/4V$, $c_4 = n_4/V$. The different species interact with reactions



The equilibrium concentrations, assuming equal probabilities of each type of k -mer, and small ϕ so the entropy of α units of i -mers is $\approx \alpha \log c_i$, must therefore satisfy

$$\begin{aligned}
 2 \log c_1 &= \log c_2 - \delta, \\
 \log c_1 + \log c_2 - \delta &= \log c_3 - 2\delta \\
 2 \log c_2 - 2\delta &= \log c_4 - 4\delta, \\
 \log c_3 + \log c_1 - 2\delta &= \log c_4 - 4\delta
 \end{aligned}$$

Solving gives

$$c_1 = e^{-\delta} c_4^{1/4}, \quad c_2 = e^{-\delta} c_4^{1/2}, \quad c_3 = e^{-\delta} c_4^{3/4}. \tag{A2}$$

The equilibrium equations are completed using conservation of mass, $(4c_1 + 4 \cdot 2c_2 + 4 \cdot 3c_3 + 4c_4)V = 4N_c$, or

$$4c_1 + 8c_2 + 12c_3 + 4c_4 = \phi, \tag{A3}$$

which after substituting for c_1, c_2, c_3 leads to

$$c_4^{1/4} + 2c_4^{1/2} + 3c_4^{3/4} + c_4 e^\delta = e^\delta \phi/4. \tag{A4}$$

This equation may be solved numerically for c_4 , given δ, ϕ . We develop an approximation valid for high yield (large c_4) momentarily.

Now suppose we wish to form a 4^k -square using hierarchical interactions. The system must first form 4-squares; therefore we must similarly ask which value of $\delta = \delta_1$ makes these 4-squares have high yield, *before* we turn on the hierarchical interactions (i.e. assuming $\delta_2 = \delta_3 = \dots = 0$). The difference from a system of pure 4-squares is that now there are 4^{k-1} distinct copies of each 4-square, so the equation for mass conservation (A3) is replaced by

$$4c_1 + 8c_2 + 12c_3 + 4c_4 = \frac{\phi}{4^{k-1}} \quad (\text{A5})$$

because the overall concentration of each type of monomer is reduced by a factor of 4. Therefore, the concentration $c_4 = n_4/4^{k-1}V$ satisfies (A4), but with $\phi \rightarrow \phi/4^{k-1}$.

When the yield $y_1^{(k)} = 4^k c_4/\phi$ is high, we may obtain a perturbative solution to (A5) by letting $y_1^{(k)} = 1 - \Delta_4^{(k)}$ with $\Delta_4^{(k)} \ll 1$. At low density where $c_4 \ll 1$, we must have $c_1 \gg c_2 \gg c_3$, so we drop c_2, c_3 . Because of the high yield assumption, $c_4 \gg c_1$, so we only include the perturbation in c_4 , making the approximations $c_4 \approx (1 - \Delta_4^{(k)})\phi/4^k$, $c_1 \approx (\phi/4^k)^{1/4}$. Solving (A5) using these approximations gives

$$\Delta_4^{(k)} \approx e^{-\delta} \left(\frac{\phi}{4^k} \right)^{-3/4}. \quad (\text{A6})$$

This allows us to approximately solve for the interaction energy required to obtain a desired yield:

$$\delta \approx k \frac{3}{4} \log 4 - \frac{3}{4} \log \phi - \log \Delta_4^{(k)}. \quad (\text{A7})$$

Appendix B: Kinetics of forming a 4-square

We may solve for the time-dependent concentrations of 4-squares by solving nonlinear ODEs corresponding to the different sub-reactions involved in forming a 4-square. We consider the reactions (A1), and assume (i) infinite volume at fixed volume fraction (ii) the system is well-mixed, and (iii) the initial concentrations of each sub-type of fragment are the same (monomer, dimer, trimer). Then standard methods give the system of reaction equations

$$\begin{aligned} \frac{dc_1}{dt} &= -2k_{11}c_1^2 + 2k_2^{\text{off}}c_2 - 2k_{21}c_1c_2 + 2k_3^{\text{off}}c_3 - k_{31}c_3c_1 + k_{43}^{\text{off}}c_4 \\ \frac{dc_2}{dt} &= k_{11}c_1^2 - k_2^{\text{off}}c_2 - 2k_{21}c_1c_2 + 2k_3^{\text{off}}c_3 - k_{22}c_2^2 + k_{42}^{\text{off}}c_4 \\ \frac{dc_3}{dt} &= 2k_{21}c_1c_2 - 2k_3^{\text{off}}c_3 - k_{31}c_3c_1 + k_{43}^{\text{off}}c_4 \\ \frac{dc_4}{dt} &= 4k_{31}c_3c_1 - 4k_{43}^{\text{off}}c_4 + 2k_{22}c_2^2 - 2k_{42}^{\text{off}}c_4. \end{aligned} \quad (\text{B1})$$

Here $k_{(\cdot)}$ represent binding rates and $k_{(\cdot)}^{\text{off}}$ represent unbinding rates. These equations can be shown to conserve total mass, $4c_1 + 8c_2 + 12c_3 + 4c_4$.

We choose the binding rates to be proportional to the sum of the species' diffusion coefficients:

$$\begin{aligned} k_{11} &= k_0 \times 2D_1 & (1 + 1 \rightarrow 2) \\ k_{21} &= k_0 \times (D_1 + D_2) & (2 + 1 \rightarrow 3) \\ k_{22} &= k_0 \times 2D_2 & (2 + 2 \rightarrow 4) \\ k_{31} &= k_0 \times (D_1 + D_3) & (3 + 1 \rightarrow 4) \end{aligned}$$

where D_1 is the diffusion coefficient of a monomer, and $D_2 = D_1/(3/2)$ is the diffusion coefficient of a 2-mer in the wide direction, and $D_3 = D_1/(1 + \sqrt{2}/3)$ is the diffusion coefficient of a 3-mer, in both directions. The base rate (if comparing with simulations) is $k_0 = 0.25$; this accounts for the directionality of the interactions, since particles can only bind if they collide in one of 4 possible orientations.

The unbinding rates are chosen to satisfy detailed balance, as

$$k_2^{\text{off}} = k_{11}e^{-\delta} \quad (2 \rightarrow 1 + 1)$$

$$k_3^{\text{off}} = k_{21}e^{-\delta} \quad (3 \rightarrow 1 + 2)$$

$$k_{42}^{\text{off}} = k_{22}e^{-2\delta} \quad (4 \rightarrow 2 + 2)$$

$$k_{43}^{\text{off}} = k_{31}e^{-2\delta} \quad (4 \rightarrow 3 + 1)$$

We solved (B1) numerically to find $\delta_{\text{opt}}(t)$, the interaction parameter δ_1 that maximizes the concentration $c_4(t)$ at fixed t , and the corresponding value of the optimal yield, $y_4^{\text{opt}}(t) = c_4(t)/\rho$, at fixed volume fraction $\phi = 0.05$. We performed the computations in Julia using packages DifferentialEquations, SciMLSensitivity, OptimJL, to solve the equations numerically, compute the gradient of $c_4(t)$ using automatic differentiation, and find the optimal parameter values using the BFGS algorithm. Fig. 3 shows a clear scaling of the optimal energy $e\delta_{\text{opt}}(t) \sim t^{0.91}$, and of the optimal yield $1 - y_4^{\text{opt}}(t) \propto t^{-0.97}$. These scalings are consistent with our predictions from (2),(3).

Appendix C: Additional figures: additional data, and finite-size effects

This section collects additional figures to support our claims in the main text.

1. A system of $n = 1024$ -squares assembling

Figure 13 shows snapshots of a system of 1024-squares assembling. Computational limitations mean we can only consider 2 copies of this system, however it is notable that we achieve very high assembly yields.

2. Finite size effects

We tested the effect of simulating a finite number of copies of each target square. We ran simulations of N_c copies of a 64-square with hierarchical interactions and with different values of N_c , repeated $N_r = 128/N_c$ times to obtain sufficient statistics. The yields are shown in Figure 14. This figure shows that finite-size effects tend to increase the yield, especially at the smallest values of copy size, $N_c \leq 4$, where the yield is significantly higher for small δ_1 . For $N_c = 2$ with larger δ_1 , the yield drops steeply.

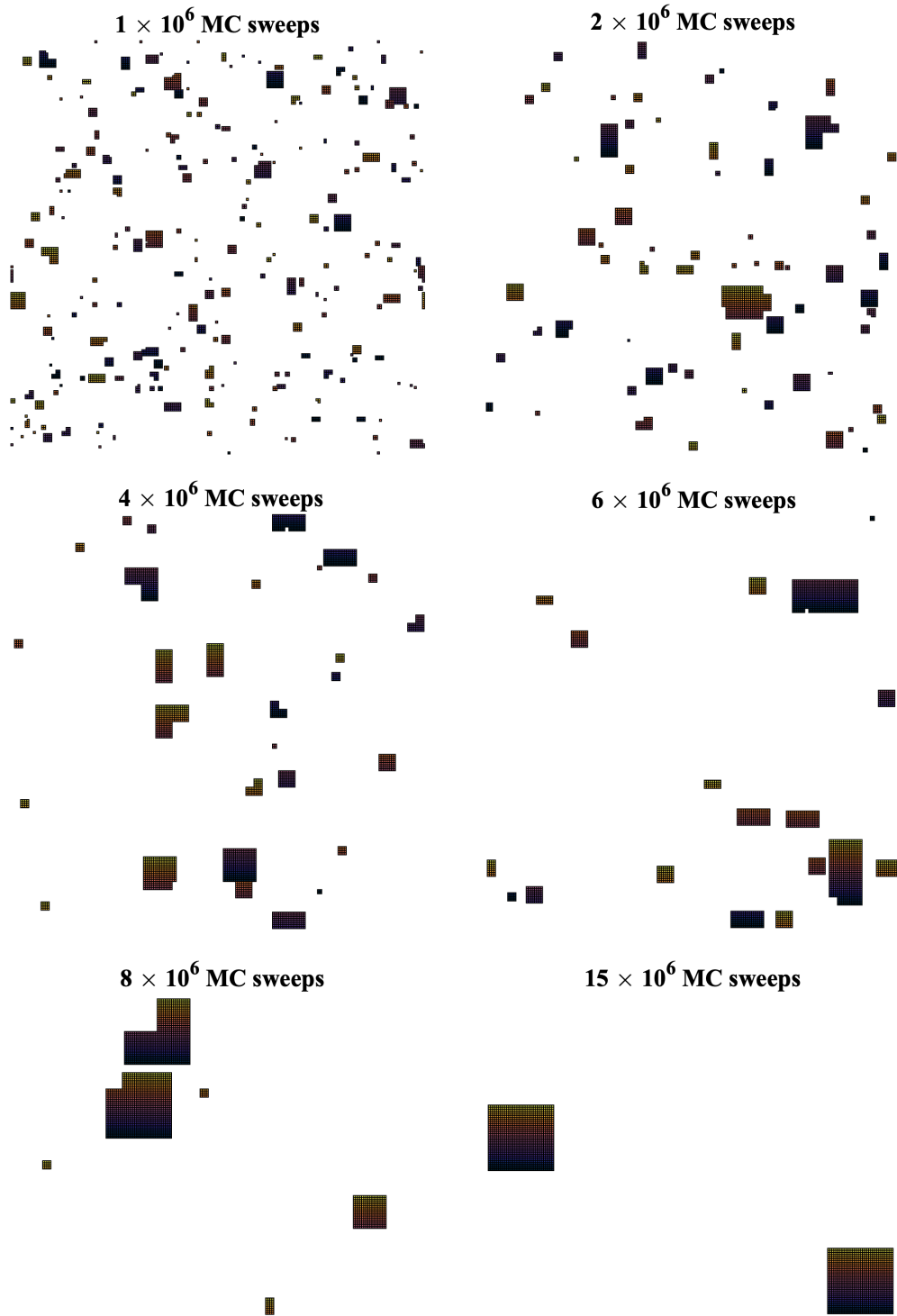


FIG. 13. Snapshots of two copies of a 1024-square assembling, using hierarchical interactions with $\delta_1 = 10$.

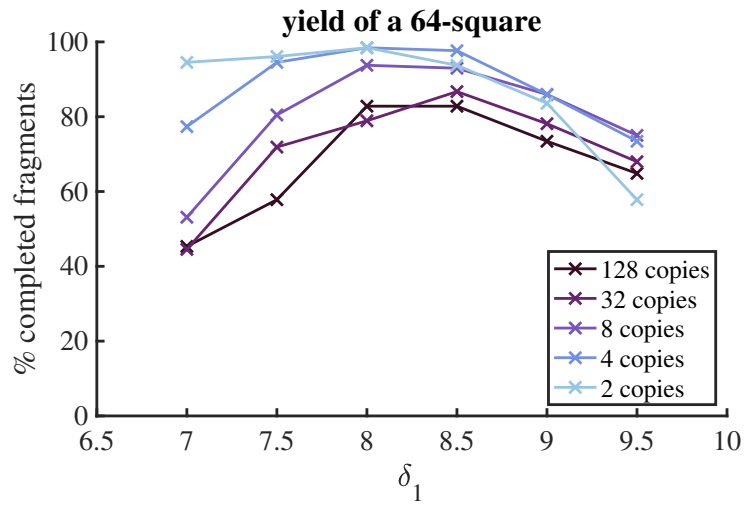


FIG. 14. Testing finite size effects in simulations of a 64-square with hierarchical interactions, at various values of δ_1 . The simulations consider N_c copies of a 64-square, with values of N_c shown in the legend, and with statistics averaged over N_r independent realizations chosen such that there are a total of $N_c N_r = 128$ total copies simulated for each choice of parameters.